



CHORUS

This is the accepted manuscript made available via CHORUS. The article has been published as:

Tunable Layer Circular Photogalvanic Effect in Twisted Bilayers

Yang Gao, Yinhan Zhang, and Di Xiao

Phys. Rev. Lett. **124**, 077401 — Published 19 February 2020

DOI: [10.1103/PhysRevLett.124.077401](https://doi.org/10.1103/PhysRevLett.124.077401)

Tunable Layer Circular Photogalvanic Effect in Twisted Bilayers

Yang Gao, Yinhan Zhang, and Di Xiao

Department of Physics, Carnegie Mellon University, Pittsburgh, PA 15213, USA

(Dated: January 9, 2020)

We develop a general theory of the layer circular photogalvanic effect (LCPGE) in quasi two-dimensional chiral bilayers, which refers to the appearance of a polarization-dependent, out-of-plane static dipole moment induced by circularly polarized light. We elucidate the geometric origin of the LCPGE as two types of interlayer coordinate shift weighted by the quantum metric tensor and the Berry curvature, respectively. As a concrete example, we calculate the LCPGE in twisted bilayer graphene, and find that it exhibits a resonance peak whose frequency can be tuned from visible to infrared as the twisting angle varies. The LCPGE thus provides a promising route towards frequency-sensitive, circularly-polarized light detection, particularly in the infrared range.

Recent years have seen a surge of interest in twisted van der Waals heterostructures consisting of atomically thin crystal layers. From a structural point of view, twisted layers are interesting because not only are they chiral, but their chirality can be readily controlled by varying the twisting angle [1]. For example, bilayers with opposite twisting angles are mirror images of each other, therefore they possess opposite chirality. This structural flexibility makes twisted van der Waals heterostructures a versatile platform for investigating chirality-dependent phenomena. One such example is the surprisingly strong circular dichroism reported in twisted bilayer graphene at large twisting angles [1–5].

In this Letter, we explore the consequence of structural chirality of twisted van der Waals bilayers in nonlinear optical effects. We show that a static, out-of-plane dipole moment can be induced by circularly polarized light at normal incidence [Fig. 1(a)], which we refer to as the layer circular photogalvanic effect (LCPGE). We first derive a general expression of the LCPGE coefficient, valid for any quasi two-dimensional chiral bilayers. The LCPGE has an elegant geometric interpretation: it consists of two types of interlayer coordinate shift, weighted by the quantum metric tensor and the Berry curvature, respectively. In this regard, the LCPGE is distinctively different from the bulk CPGE [6–9], and resembles more of the shift current [10–15].

We then demonstrate the tunability of the LCPGE in twisted bilayer graphene. We find that the LCPGE signal exhibits a resonance peak determined by three factors: the enhanced density of states, the quantum metric tensor, and the finite interlayer coordinate shift. The peak frequency can be tuned from visible to infrared with decreasing twisting angle and, at the same time, its magnitude increases sharply (Fig. 4). For example, at about 2° twisting angle, for a circularly polarized light at 250 meV with a power of $1 \text{ mW}/\mu\text{m}^2$, the induced voltage difference between the two layers is found to be $20 \mu\text{V}$. These properties make the LCPGE in twisted bilayer graphene a promising candidate towards frequency-sensitive, circularly-polarized light detection in the infrared range.

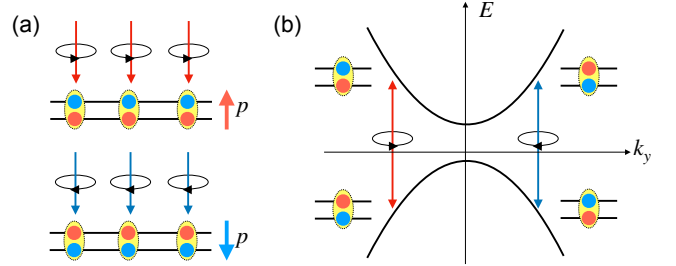


FIG. 1. (a) Schematic illustration of the LCPGE. Circularly polarized light induces a static out-of-plane dipole, whose direction flips when the circular polarization of light is reversed. Red and blue disks stand for negative and positive charges, respectively. (b) Origin of the LCPGE. The incident light excites an electron from the valence band to the conduction band, while simultaneously causes a change in the dipole moment. Such a transition process is dependent on the light chirality through the geometric factor β_G in Eq. (5).

General Theory.—Let us consider a generic quasi two-dimensional chiral bilayer, i.e., its structure lacks any mirror plane and inversion center. The out-of-plane dipole moment is represented by the operator $\hat{p} = -e\sigma_z$, where the Pauli matrix σ_z operates in the layer index subspace and we have set the distance between the two layers to be unity. We further assume that the system has an in-plane C_{2x} axis, as is the case of twisted bilayer graphene. The C_{2x} symmetry forbids the existence of the out-of-plane dipole in equilibrium.

Under normal incidence, the dipole $\langle \hat{p} \rangle$ has the following static component

$$\langle \hat{p} \rangle = \chi_{ij}(\omega, -\omega) E_i(\omega) E_j(-\omega), \quad (1)$$

where $E_i(\pm\omega) = \pm i\omega A_i(\pm\omega)$ with $\mathbf{A}(\pm\omega)$ being the Fourier components of the vector potential with frequencies $\pm\omega$. We can decompose the response coefficient χ_{ij} into a symmetric part χ_{ij}^s and an antisymmetric part χ_{ij}^{as} . Since \hat{p} is odd under C_{2x} , χ_{ij}^s can only have off-diagonal components. In addition, if there is a more-than-two-fold rotational axis in the z -direction, χ_{ij}^s has to vanish. In contrast, χ_{ij}^{as} transforms as a pseudoscalar, i.e., it is

invariant under rotation, but flips sign under mirror reflection and space inversion. Therefore χ_{ij}^{as} is allowed as long as the crystal structure is chiral.

The antisymmetric tensor χ_{ij}^{as} directly couples to the handedness of light. This can be seen by recasting the polarization $\langle \hat{p} \rangle$ due to χ_{ij}^{as} into the following form

$$\langle \hat{p} \rangle = \beta [iE_x(\omega)E_y(-\omega) - iE_y(\omega)E_x(-\omega)], \quad (2)$$

where $\beta = -i\chi_{xy}^{\text{as}}$. The expression inside the square bracket is proportional to the fourth Stokes parameter which reflects the circular polarization of light.

The LCPGE coefficient β can be obtained as follows. In the presence of an incident light, the Hamiltonian reads $\hat{H} = \hat{H}_0 + e\hat{\mathbf{v}} \cdot \mathbf{A}$ with \hat{H}_0 the unperturbed Hamiltonian. Note that for nonlinear responses, the second order perturbative Hamiltonian $\hat{H}^{(2)} = \frac{1}{2}\hat{\Gamma}_{ij}A_iA_j$ is usually needed, with $\hat{\Gamma}_{ij} = \partial\hat{v}_j/\partial p_i$ being the Hessian matrix. However, this term does not contribute to χ_{ij}^{as} as the matrix element of $\hat{\Gamma}_{ij}$ always vanishes upon taking the antisymmetrization of the index i and j .

We then solve the change to the density matrix up to second order and use it to calculate $\langle \hat{p} \rangle$. The details are left to the Supplemental Material [16]. Let $\beta = -e^2\beta_0/\omega^2$; we find that β_0 is given by a summation over three band indices,

$$\beta_0 = -i \sum_{\ell, m, n} \int \frac{d\mathbf{k}}{(2\pi)^2} \frac{(v_y)_{m\ell}(v_x)_{\ell n} - (x \leftrightarrow y)}{\omega_{nm} + i\eta_1} \times (G_{\ell n} + G_{m\ell})p_{nm}, \quad (3)$$

where $(v_\alpha)_{m\ell}$ and p_{nm} are the velocity and dipole matrix element in the band basis, respectively, $\omega_{nm} = \varepsilon_n - \varepsilon_m$, and $G_{\ell n} = (f_\ell - f_n)/(\omega_{\ell n} - \omega - i\eta_2) - (f_\ell - f_n)/(\omega_{\ell n} + \omega - i\eta_2)$ with f_n being the Fermi-Dirac distribution. Two phenomenological parameters η_1 and η_2 have been introduced to take into account of various relaxation processes.

Geometric origin.—We now reveal the geometric origin of the LCPGE. We first show that the intraband contributions ($\varepsilon_n = \varepsilon_m$) in Eq. (3) vanishes. For non-degenerate bands, $\varepsilon_n = \varepsilon_m$ implies that $n = m$. In this case, $(v_y)_{m\ell}(v_x)_{\ell m} - (x \leftrightarrow y)$ is proportional to the band-resolved Berry curvature $(\Omega_z)_{m\ell}$ [see Eq. (6) below], which is odd under time-reversal. Since both the band energy ε_n and the dipole moment p_{mm} are even under time-reversal, the integral in Eq. (3) vanishes for intraband contributions. One can prove that the same conclusion also holds for the degenerate case.

Next we consider the interband contributions ($\varepsilon_n \neq \varepsilon_m$). If $\eta_1 \ll |\omega_{nm}|$, we can approximate $\omega_{nm} + i\eta_1 \approx \omega_{nm}$. It is convenient to introduce an auxiliary Hamiltonian $\hat{H}_0(\lambda) = \hat{H}_0 + \lambda\hat{p}$ with λ being the layer potential difference. We can then write the interband dipole moment as $p_{nm} = \langle u_n | \hat{p} | u_m \rangle = \omega_{nm} \langle \partial_\lambda u_n | u_m \rangle$, where $e^{i\mathbf{k} \cdot \mathbf{r}} | u_n(\lambda) \rangle$ is the λ -dependent Bloch function of $\hat{H}_0(\lambda)$.

TABLE I. Transformation properties of quantities in Eq. (5).

	Tr g_{ij}	Ω_z	R_{as}	R_s
$\mathcal{M}_{x,y}$	+	-	-	+
\mathcal{M}_z	+	+	-	-
\mathcal{I}	+	+	-	-

Insert this expression into Eq. (3) and let $\lambda \rightarrow 0$ in the end. We find that, in the clean limit ($\eta_2 \rightarrow 0$), β_0 can be written as a summation over only two band indices [16],

$$\beta_0 = \lim_{\lambda \rightarrow 0} \sum_{\ell, n} \sum_{\xi=\pm 1} \int \frac{d\mathbf{k}}{(2\pi)^2} \omega_{\ell n}^2 (f_n - f_\ell) \xi \delta(\omega_{n\ell} + \xi\omega) \beta_G. \quad (4)$$

In Eq. (4), we have separated the contribution to β_0 into a spectral part, $(f_n - f_\ell)\delta(\omega_{n\ell} \pm \omega)$, whose integration gives rise to the joint density of states, and a geometric part $\omega_{\ell n}^2 \beta_G$ with β_G given by

$$\beta_G = (\text{Tr } g_{ij})_{n\ell} (R_{\text{as}})_{n\ell} - (\Omega_z)_{n\ell} (R_s)_{n\ell}. \quad (5)$$

We now explain the various terms in β_G . The quantities $(\Omega_z)_{n\ell}$ and $(g_{ij})_{n\ell}$, defined by

$$(\Omega_z)_{n\ell} = -2\text{Im}[\langle u_n | i\partial_{k_x} u_\ell \rangle \langle u_\ell | i\partial_{k_y} u_n \rangle], \quad (6)$$

$$(g_{ij})_{n\ell} = \text{Re}[\langle u_n | i\partial_{k_i} u_\ell \rangle \langle u_\ell | i\partial_{k_j} u_n \rangle], \quad (7)$$

have the meaning of the band-resolved Berry curvature and quantum metric tensor, respectively. They have the property that summing over one band index will recover the full Berry curvature and quantum metric in the other band, i.e., $\sum_{\ell \neq n} (\Omega_z)_{n\ell} = (\Omega_z)_n$ and $\sum_{\ell \neq n} (g_{ij})_{n\ell} = (g_{ij})_n$ [17, 18].

The quantities $(R_{\text{as}})_{n\ell}$ and $(R_s)_{n\ell}$ are given by $(R_{\text{as},s})_{n\ell} = \frac{1}{2}[(R_+)_{n\ell} \mp (R_-)_{n\ell}]$ with

$$(R_\pm)_{n\ell} = \partial_\lambda (\phi_\pm)_{n\ell} - (a_\lambda)_n + (a_\lambda)_\ell, \quad (8)$$

where $(\phi_\pm)_{n\ell} = \arg(v_\pm)_{n\ell}$ is the phase of the velocity matrix element $v_\pm = v_x \pm iv_y$, and $(a_\lambda)_n = \langle u_n | i\partial_\lambda | u_n \rangle$ is the Berry connection. Note that due to the appearance of a_λ , both R_\pm and $R_{\text{as},s}$ are independent of the $U(1)$ gauge transformation of the Bloch state.

One immediately recognizes that the expression for R_\pm shares a striking similarity with the coordinate shift in the shift current expression, with the latter given by $\mathbf{R}_{n\ell} = \partial_{\mathbf{k}} \phi_{n\ell} - (\mathbf{a}_{\mathbf{k}})_n + (\mathbf{a}_{\mathbf{k}})_\ell$ [10–14], where $\phi_{n\ell} = \arg(v_x)_{n\ell}$ and $(\mathbf{a}_{\mathbf{k}})_n = \langle u_n | i\partial_{\mathbf{k}} | u_n \rangle$. Since λ is conjugate to the dipole moment p , we can interpret R_\pm as the interlayer coordinate shift, which has the desired property that it flips sign under mirror reflection \mathcal{M}_z with respect to the xy -plane. Thus the LCPGE can be interpreted in terms of geometric quantities defined in the (\mathbf{k}, λ) parameter space: it consists of two types of interlayer coordinate shifts, weighted by the band resolved quantum metric and the Berry curvature, respectively.

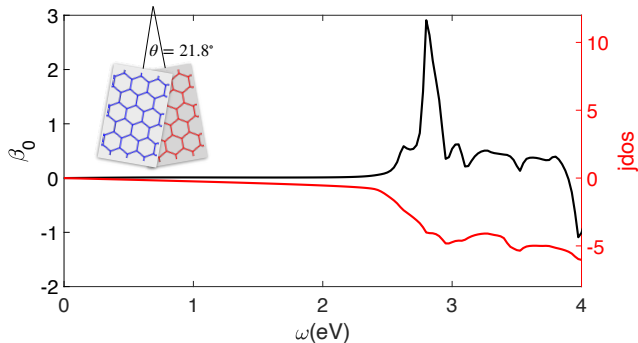


FIG. 2. The LCPGE coefficient β_0 and the joint density of states (jdos) in twisted bilayer graphene with twisting angle $\theta = 21.8^\circ$. β_0 is in unit of e/\hbar^2 . The joint density of states is in units of $1/3a^2$ per electron volts with a being the lattice constant of the bilayer graphene. The phenomenological relaxation parameters are chosen as $\eta_1 = \eta_2 = 0.02$ eV. The Fermi level is taken at the Dirac point.

The two-band formula in Eq. (4) and Eq. (5) also provides a simple picture of the LCPGE as shown in Fig. 1(b). Let us write the integrand of Eq. (4) as

$$\omega_{\ell n}^2 \beta_G = (W_+)_{n\ell}(p_+)_{n\ell} - (W_-)_{n\ell}(p_-)_{n\ell}, \quad (9)$$

where $(W_{\pm})_{n\ell} = \omega_{\ell n}[(\text{Tr}g_{ij})_{n\ell} \mp (\Omega_z)_{n\ell}]$ is nothing but the oscillator strength of the left and right circularly polarized light for the transition from n -th to ℓ -th band [19], and $(p_{\pm})_{n\ell} = \omega_{\ell n}(R_{\pm})_{n\ell}$ describes the change in the dipole moment that occurs as an electron absorbs a chiral photon. Therefore the LCPGE directly measures the difference in the induced dipole moment when the electrons are excited by left and right circularly polarized light.

The geometric factor β_G is fully compatible with the point-group symmetry requirement of the LCPGE. The Berry curvature transforms as a pseudovector, and the trace of the quantum metric tensor $\text{Tr}g_{ij}$ transforms as a scalar. The phase factor ϕ_+ and ϕ_- transform in the following way: $\phi_+ \rightarrow \pi + \phi_-$ and $\phi_- \rightarrow \pi + \phi_+$ under \mathcal{M}_x , $\phi_+ \rightarrow \phi_-$ and $\phi_- \rightarrow \phi_+$ under \mathcal{M}_y , and $\phi_+ \rightarrow \phi_+ + \pi$ and $\phi_- \rightarrow \phi_- + \pi$ under inversion. Finally, $\partial_\lambda \rightarrow -\partial_\lambda$ under \mathcal{M}_z and inversion. The transformation properties of the geometric quantities in Eq. (5) are summarized in Table I. We can see that β_G is odd under chirality reversal operations such as inversion and mirror operations.

Before closing this section, we wish to remark that even though our LCPGE shares the same symmetry requirement as the out-of-plane component of the bulk CPGE, their geometric origins are completely different. The bulk CPGE is determined by the Berry curvature dipole [6–9], while our LCPGE resembles more of the shift current [10–15], and depends on both the Berry curvature and the quantum metric tensor.

Twisted bilayer graphene.—We now apply our theory of the LCPGE to twisted bilayer graphene. We begin

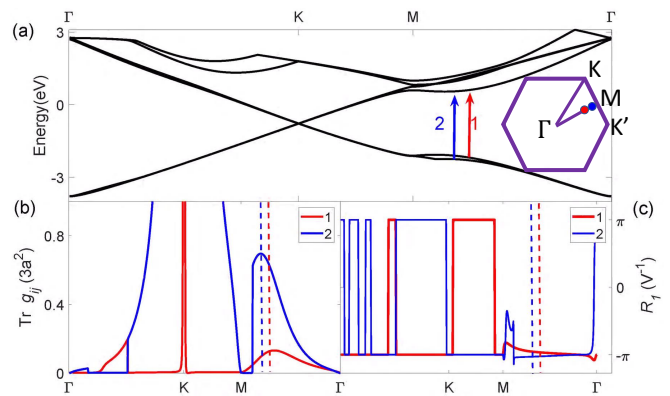


FIG. 3. Geometric origin of the peak at 2.8 eV in Fig. 2. We plot the band spectrum in (a), the quantum geometric tensor ($\text{Tr}g_{ij})_{n\ell}$ in (b) and the interlayer coordinate shift R_{as} in (c), along the high symmetry line shown in black in the inset of (a). In (a), we include the spectrum from 13-th to 18-th band. The red and blue arrows in (a) show the optical transition with a photon energy 2.8 eV, which are also shown as dots in the inset plot of the Brillouin zone. For $(\text{Tr}g_{ij})_{n\ell}$ and $(R_{as})_{n\ell}$, we consider the quantities with $n = 14$ and $\ell = 15$, and with $n = 13$ and $\ell = 15$, which correspond to the red and blue transitions shown in (a). The blue and red dashed lines in (b) and (c) are at the same position in the Brillouin zone with the blue and red arrows in (a).

with an AB stacked bilayer graphene, then twist one of the layers around a point where the top and bottom lattice points overlap. At arbitrary twisting angle except when $\theta = n\pi/3$, the resulting structure, whether commensurate or incommensurate, always respects the chiral D_3 or D_6 group [20–23].

The twisted bilayer graphene is modeled using a tight-binding Hamiltonian at commensurate angles, following the procedure outlined in Ref. [24]. To see the characteristic behavior of the LCPGE, we choose the twisting angle $\theta = 21.8^\circ$, which contains 28 atoms in the unit cell. We plot β_0 as a function of the photon energy in Fig. 2, calculated using Eq. (3). We can see that below a threshold photon energy, β_0 is approximately zero. It then develops a sharp peak at around 2.8 eV, followed by finite but oscillating behavior.

Three factors conspire to render the appearance of the resonance peak in β_0 : a large joint density of states, a peak in the geometric tensor ($\text{Tr}g$), and a finite shift between layers (R_{as}). To demonstrate this, we first plot the joint density of states (jdos) in conjunction with β_0 in Fig. 2, which is defined by

$$\text{jdos} = \text{Im} \int \frac{d\mathbf{k}}{(2\pi)^2} \sum_{m \neq n} \frac{f_m - f_n}{\omega_{mn} - \omega - i\eta_2}. \quad (10)$$

In the flat region where β_0 is close to zero, the joint density of states varies linearly, demonstrating the typical behaviour of the two-dimensional Dirac point. As the joint density of states rises sharply, so is β_0 . However, the

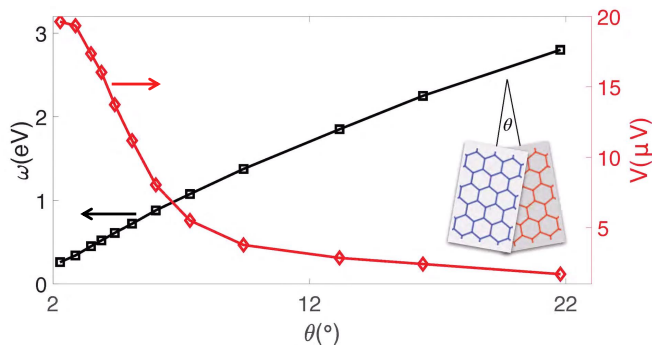


FIG. 4. The peak position (black) and the corresponding potential difference (red) generated by the LCPGE at different twisting angles. We have assumed a laser power $1 \text{ mW}/\mu\text{m}^2$.

first peak of β_0 does not coincide with that of the joint density of states, although there are synchronized but much weaker peaks at higher energies. This shows that even though the increased density of states contributes to the enhanced β_0 , it is not the only factor.

We now reveal the geometric origin of the peak. In Fig. 3(a), we plot the energy bands along high symmetry lines as shown in the inset of Fig. 3(a) in the Brillouin zone of the supercell and label the optical transition responsible for the peak in β_0 . We can see that the band dispersion around the Dirac point ceases to be linear at the M - Γ line that bisects the two Dirac points. On this line a local band edge is developed, rendering a relatively flat region, which hosts the optical transition for the peak in β_0 and is responsible for the sharp rise of the joint density of states shown in Fig. 2. This will provide ample initial and final states for the optical transitions and hence amplify the magnitude of β_0 .

In Fig. 3(b) and (c), we plot the quantum metric tensor and the layer shift R_{as} corresponding to the two transitions labeled in Fig. 3(a). We find that near both transitions, the shift R_{as} is close to $-\pi$ without much variation, while the quantum metric tensor experiences peaks which eventually leads to the peak in β_0 . This turns out to be the dominant geometric contribution to the LCPGE peak since we have found that there is no contribution from the second term in Eq. (5) as the Berry curvature vanishes for the two bands involved in the optical transition. This is due to the 2D Dirac point with a vanishing band gap. We expect this contribution to appear in twisted transition metal dichalcogenides.

The appearance of the resonance peak in the LCPGE is a general feature of twisted bilayer graphene. As shown in Fig. 4, the resonance frequency varies from visible to infrared as the twisting angle decreases from 22° to 2° . This is expected because the twisting angle controls the energy where the Dirac cones from the top and bottom layer intersect, at which the LCPGE becomes appreciable. Figure 4 also shows the induced voltage difference

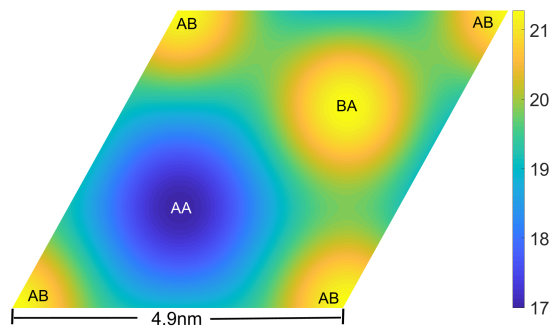


FIG. 5. The real-space resolved layer potential difference (μV) induced by the LCPGE in the moire supercell at the twisting angle $\theta = 2.87^\circ$ and the peak frequency $\omega = 0.34 \text{ eV}$.

between the two layers, calculated from $V = \langle p \rangle / \epsilon_0$ with ϵ_0 the vacuum permittivity. We can see that the voltage increases considerably with decreasing twisting angles, owing to the decreasing peak frequencies and the prefactor $1/\omega^2$ in β . The LCPGE signal can be further enhanced in multilayer chiral stacked structures.

Finally, we plot the real-space map of the induced layer potential in Fig. 5 at $\theta = 2.87^\circ$ (details given in the Supplemental Materials [16]). We see that the potential is almost uniform throughout the entire unit cell with moderate variation, with minima near the AA-stacked region and maxima near the AB/BA-stacked region. Note that the potential never changes sign. Therefore if there is moderate lattice relaxation or strain, we do not expect any cancellation effect, and the LCPGE should be a relatively robust effect against relaxation. On the other hand, it has been shown that for twisting angle smaller than 2° , the lattice relaxation changes the band structure significantly [25], and we leave the LCPGE in this situation for future study.

In general, a twisted bilayer is specified by both its twist angle and relative shift between the two layers. We have found that at $\theta = 21.8^\circ$, the LCPGE signal shows some, but not strong dependence on the relative shift (See Fig. S2 in the Supplemental Materials [16]). This behavior is similar to that in the circular dichroism in the same structure [5].

To experimentally measure the induced dipole moment, a possible approach is the compressibility measurement using the capacitance method [26, 27] or a scanning single electron transistor [28]. In the former method, a $10 \mu\text{V}$ voltage across bilayers can translate to a sizable gate voltage on the order of mV. In the latter method, μV voltage is directly accessible [28]. Interaction with substrate can break the C_{2x} symmetry assumed earlier and induce a dipole moment in equilibrium. In experiments, this can be discounted by taking the difference between the signals with and without light, or lights with opposite circular polarization.

In summary, we have studied the layer circular photo-

galvanic effect in quasi-two-dimensional chiral materials, and revealed its geometric origin. This geometric view offers a route to designing nonlinear optical chiral materials. The calculated LCPGE coefficient in twisted bilayer graphene exhibits a highly tunable resonance peak as a function of the twisting angle and photo energy, which may be useful for frequency-sensitive, circularly-polarized light detection, particularly in the infrared range.

We acknowledge useful discussions with Dmitri Basov, Kenneth Burch, Ben Hunt, Abhay Pasupathy, Dong Sun, and Suyang Xu. We also thank Chong Wang for his suggestions for code optimization. This work is mainly supported by the Department of Energy, Basic Energy Sciences, Grant No. DE-SC0012509. The modeling of the moire superlattice is supported by the Department of Energy, Basic Energy Sciences, Pro-QM EFRC (DE-SC0019443). D.X. also acknowledges the support of a Simons Foundation Fellowship in Theoretical Physics.

-
- [1] Cheol-Joo Kim, A. Sánchez-Castillo, Zack Ziegler, Yui Ogawa, Cecilia Noguez, and Jiwoong Park, “Chiral atomically thin films,” *Nat. Nanotech.* **11**, 520 (2016).
- [2] E. S. Morell, L. Chico, and L. Brey, *2D Mater.* **4**, 035015 (2017).
- [3] T. Stauber, T. Low, and G. Gómez-Santos, “Chiral response of twisted bilayer graphene,” *Phys. Rev. Lett.* **120**, 046801 (2018).
- [4] T. Stauber, T. Low, and G. Gómez-Santos, “Linear response of twisted bilayer graphene: Continuum versus tight-binding models,” *Phys. Rev. B* **98**, 195414 (2018).
- [5] Zachariah Addison, Jiwoong Park, and E. J. Mele, “Twist, slip, and circular dichroism in bilayer graphene,” *Phys. Rev. B* **100**, 125418 (2019).
- [6] J. E. Moore and J. Orenstein, “Confinement-induced berry phase and helicity-dependent photocurrents,” *Phys. Rev. Lett.* **105**, 026805 (2010).
- [7] E. Deyo, L.E. Golub, E.L. Ivchenko, and B. Spivak, “Semiclassical theory of the photogalvanic effect in non-centrosymmetric systems,” arXiv: 0904.1917 (2009).
- [8] Inti Sodemann and Liang Fu, “Quantum nonlinear hall effect induced by berry curvature dipole in time-reversal invariant materials,” *Phys. Rev. Lett.* **115**, 216806 (2015).
- [9] Fernando de Juan, Adolfo G. Grushin, Takahiro Morimoto, and Joel E Moore, “Quantized circular photogalvanic effect in weyl semimetals,” *Nat. Commun.* **8**, 15995 (2017).
- [10] Wolfgang Kraut and Ralph von Baltz, “Anomalous bulk photovoltaic effect in ferroelectrics: A quadratic response theory,” *Phys. Rev. B* **19**, 1548 (1979).
- [11] Ralph von Baltz and Wolfgang Kraut, “Theory of the bulk photovoltaic effect in pure crystals,” *Phys. Rev. B* **23**, 5590 (1981).
- [12] J. E. Sipe and A. I. Shkrebtii, *Phys. Rev. B* **61**, 5337 (2000).
- [13] B. I. Sturman and V. M. Fridkin, *The photovoltaic and photorefractive effects in noncentrosymmetric materials* (Gordon and Breach Science Publishers, Philadelphia, 1992).
- [14] T. Morimoto and N. Nagaosa, “Topological nature of nonlinear optical effects in solids,” *Sci. Adv.* **2**, e1501524–e1501524 (2016).
- [15] Xu Yang, Kenneth Burch, and Ying Ran, “Divergent bulk photovoltaic effect in weyl semimetals,” arXiv: 1712.09363 (2017).
- [16] “Supplemental material,” See Supplemental Material.
- [17] J. P. Provost and G. Vaille, “Riemannian structure on manifolds of quantum states,” *Comm. Math. Phys.* **76**, 289 (1980).
- [18] M. V. Berry, “Quantal phase factors accompanying adiabatic changes,” *Proc. R. Soc. Lond. A* **392**, 45 (1984).
- [19] Ivo Souza and David Vanderbilt, “Dichroic-sum rule and the orbital magnetization of crystals,” *Phys. Rev. B* **77**, 054438 (2008).
- [20] Jian Kang and Oskar Vafek, “Symmetry, maximally localized wannier states, and a low-energy model for twisted bilayer graphene narrow bands,” *Phys. Rev. X* **8**, 031088 (2018).
- [21] M. Angeli, D. Mandelli, A. Valli, A. Amaricci, M. Capone, E. Tosatti, and M. Fabrizio, “Emergent d6 symmetry in fully relaxed magic-angle twisted bilayer graphene,” *Phys. Rev. B* **98**, 235137 (2018).
- [22] Liujun Zou, Hoi Chun Po, Ashvin Vishwanath, and T. Senthil, “Band structure of twisted bilayer graphene: Emergent symmetries, commensurate approximants, and wannier obstructions,” *Phys. Rev. B* **98**, 085435 (2018).
- [23] Yinhan Zhang, Yang Gao, and Di Xiao, “Topological charge pumping in twisted bilayer graphene,” arXiv: 1910.09001 (2019).
- [24] Pilkyung Moon and Mikito Koshino, “Optical absorption in twisted bilayer graphene,” *Phys. Rev. B* **87**, 205404 (2013).
- [25] Nguyen N. T. Nam and Mikito Koshino, “Lattice relaxation and energy band modulation in twisted bilayer graphene,” *Phys. Rev. B* **96**, 075311 (2017).
- [26] Andrea F. Young and Leonid S. Levitov, “Capacitance of graphene bilayer as a probe of layer-specific properties,” *Phys. Rev. B* **84**, 085441 (2011).
- [27] A. F. Young, C. R. Dean, I. Meric, S. Sorgenfrei, H. Ren, K. Watanabe, T. Taniguchi, J. Hone, K. L. Shepard, and P. Kim, “Electronic compressibility of layer-polarized bilayer graphene,” *Phys. Rev. B* **85**, 235458 (2012).
- [28] J. Martin, B. E. Feldman, R. T. Weitz, M. T. Allen, and A. Yacoby, “Local compressibility measurements of correlated states in suspended bilayer graphene,” *Phys. Rev. Lett.* **105**, 256806 (2010).